Research Square

Preprints are preliminary reports that have not undergone peer review.
They should not be considered conclusive, used to inform clinical practice,
or referenced by the media as validated information.

Source-dependent epoxide depletion in graphene oxide induced by soft X-rays and low-energy electron irradiation

Enver Faella
University of L'Aquila
Daniele Capista
Leibniz Institute for High Performance Microelectronics
Luca Camilli
University of Rome Tor Vergata
Luca Lozzi
University of L'Aquila
Maurizio Passacantando
maurizio.passacantando@univaq.it

University of L'Aquila

Article

Keywords: Graphene oxide, Radiation-induced reduction, Soft X-ray irradiation, Low-energy electron irradiation, X-ray photoelectron spectroscopy

Posted Date: August 28th, 2026

DOI: https://doi.org/10.21203/rs.3.rs-10624346/v1

License: This work is licensed under a Creative Commons Attribution 4.0 International License.
Read Full License

Additional Declarations: No competing interests reported.

Abstract

The chemical response of graphene oxide (GO) to ionizing radiation depends on both its oxygen-containing functional groups and the energy-deposition characteristics of the radiation source. Here, self-supported GO sheets exposed to Mg Kα (1253.6 eV) X-rays and 500 eV electrons were investigated by X-ray photoelectron spectroscopy. C 1s and O 1s spectra reveal selective depletion of epoxide (C–O–C) groups, accompanied by increases in sp^2 carbon and hydroxyl-related components, while carbonyl and carboxyl groups remain nearly unchanged upon irradiation. For both sources, epoxide depletion follows a phenomenological saturating-exponential dependence on the estimated local absorbed dose. The characteristic dose is 140 ± 10 MGy for X-rays and 2310 ± 235 MGy for electrons, although electron-induced saturation is not experimentally reached. Electrons produce apparent faster changes with exposure time because of their higher dose rate but show significantly lower dose-normalized efficiency. Under the maximum exposure conditions, the nominal local electron dose is approximately 13 times the Mg Kα dose within the adopted K–O-derived continuous-slowing-down approximation. Thus, both sources induce qualitatively similar, epoxide-selective reduction, whereas the dose-normalized response remains strongly source dependent.

1. Introduction

Graphene oxide (GO) is a chemically modified two-dimensional carbon material consisting of graphitic sp^2 domains decorated with a variety of oxygen-containing functional groups, mainly hydroxyl, epoxide, carbonyl and carboxyl species[1–3]. The type, concentration and spatial distribution of these groups govern the hydrophilicity, interlayer spacing, electronic structure, chemical reactivity and mechanical properties of GO, and determine its transformation toward reduced graphene oxide (*r*GO)[1–4]. In particular, epoxide and hydroxyl groups are commonly associated with the basal plane of GO, whereas carbonyl and carboxyl species are preferentially located at edges and defect sites. Since reduction progressively removes or rearranges these oxygen functionalities and partially restores the conjugated sp^2 carbon network, understanding the chemical pathways involved in GO reduction is essential for applications in electronics, sensing, energy storage, membranes and biomedicine.

Several approaches have been developed to reduce GO, including chemical reduction, thermal annealing, electrochemical treatments, laser irradiation and exposure to ionizing radiation[4–7]. Among them, radiation-induced reduction is particularly attractive because it enables reagent-free, spatially controlled and exposure-dependent modification of GO without high-temperature processing or chemical reducing agents. Previous studies have shown that soft photons, electron beams and ion beams can induce oxygen removal, modify the C/O ratio and progressively restore graphitic domains in GO and *r*GO sheets[8,9]. The irradiation-induced chemical evolution of GO has also been proposed as a potential indicator of radiation exposure[8].

However, most radiation-induced reduction studies have mainly considered global indicators, such as the overall C/O atomic ratio, while the dose-dependent evolution of individual oxygen-containing functional groups has received less attention. This distinction is important because GO reduction is not necessarily a uniform deoxygenation process and different oxygen groups may exhibit different radiation sensitivities, reaction pathways and saturation behaviours. In particular, epoxide groups are chemically reactive and can undergo ring-opening reactions, making them potential preferential sites for irradiation-induced bond breaking and local rearrangement of the carbon framework[10].

X-ray photoelectron spectroscopy (XPS) is especially suitable for addressing this issue, because detailed analysis of the C 1s and O 1s core-level spectra allows the evolution of graphitic carbon, hydroxyl, epoxide, carbonyl and carboxyl components to be followed separately[11–13]. Moreover, since XPS probes only the near-surface region[14,15], the radiation response should be evaluated in terms of absorbed dose within the XPS-sensitive volume rather than only as a function of exposure time. This is particularly relevant when comparing different radiation sources, such as soft X-rays and low-energy electrons, which differ strongly in dose rate, penetration depth and energy-deposition profile.

In this work, we investigate whether soft Mg Kα X-rays (1253.6 eV) and low-energy electrons at 500 eV produce comparable changes in the individual oxygen-containing functionalities of self-supported GO sheets. The chemical evolution is monitored by detailed C 1s and O 1s XPS analysis, with particular attention to the epoxide C–O–C component as a chemically selective descriptor of irradiation-induced reduction. The response is expressed as an epoxide-depletion yield and compared as a function of irradiation time and estimated local absorbed dose. A common first-order-like saturation model is used as a phenomenological framework to analyse the data collected for the two radiation sources. This approach separates the real-time evolution from the dose-normalized chemical response and allows the influence of the source-specific interaction and near-surface energy-deposition characteristics to be assessed.

2. Materials and methods

Graphene oxide sheet preparation

Graphene oxide sheet was prepared, according to a previously reported procedure[16], using a commercial aqueous GO dispersion (Graphenea, 0.4 wt.%). The suspension was drop-cast onto a hydrophobic polished substrate and dried under ambient conditions for 12 h. The resulting self-supported GO sheets were detached from the substrate and used for irradiation experiments. The thickness of the GO sheet was estimated to be approximately 10 μm from SEM measurements of its cross-section.

Irradiation procedures

GO samples were irradiated in an ultra-high-vacuum chamber using a non-monochromatic Mg Kα X-ray source or a low-energy electron beam. The Mg Kα photon energy is 1253.6 eV. Electron irradiation was performed at a primary energy of 500 eV and a beam current of 0.17 μA. Exposure times were varied to

induce progressive surface reduction of GO. The maximum exposure times were 35 h for Mg Kα X-rays, and 2 h for 500 eV electrons. The irradiated area was approximately 1 cm^2 for the X-ray source. The nominal beam cross-section perpendicular to the electron-beam direction was 0.09 cm^2. At an incidence angle of 45° with respect to the sample surface, this corresponds to a projected sample footprint of 0.127 cm^2.

X-ray photoelectron spectroscopy

XPS measurements were performed using a PHI 1257 system operating at a base pressure of 5×10^{-10} mbar with Mg Kα X-ray source. Detailed C 1s and O 1s spectra were acquired using a hemispherical analyser. The analysed area was approximately 0.016 cm^2. Charging effects were corrected by using the binding-energy reference of Ag $3d_{5/2}$ signal at 368.3 eV of a silver paint point present on the sample surface.

Morphological and structural characterization

The morphology and crystallographic structure of the GO sheets were investigated by field-emission scanning electron microscopy using a Zeiss LEO 1530 FE-SEM and by X-ray diffraction using a Bruker D5000 diffractometer with Cu Kα radiation.

Estimation of the local absorbed dose

The absorbed dose was evaluated in the XPS-sensitive probed near-surface region as:

$$D = \frac{E_{\mathrm{abs}}}{m} \# \ (1)$$

where E_{abs} is the energy absorbed by the GO film and m is the mass of the irradiated volume. The corresponding dose rate was calculated as:

$$\dot{D} = \frac{P_{\mathrm{abs}}}{m} \# \ (2)$$

with P_{abs} the absorbed power. For Mg Kα irradiation, the absorbed power was estimated from the photon energy, photon flux density, irradiated area and the absorbed fraction of the incident photon energy in GO layer, calculated using soft X-ray attenuation data (see Supplementary Information for more details)[17]. For the case of electron irradiation, the incident beam power was calculated as $P_e = I \bullet V$, with I, the measured beam current, and V the accelerating voltage. Because the GO sheet thickness is much larger than the estimated electron range, transmission through the entire GO sheet was neglected. However, only the fraction of the incident energy nominally lost within the first 10 nm was included in the near-surface dose estimate. The electron interaction depth was estimated using the Kanaya–Okayama (K–O) range relation[18], while the fraction of electron energy nominally deposited within the XPS-sensitive depth was estimated using a K–O-derived continuous-slowing-down approximation (CSDA). Although a full Monte Carlo electron-transport simulation would be required to determine the detailed energy-

deposition profile[19–21], the K–O formalism provides a reasonable first-order estimate of the near-surface electron interaction depth. The K–O range was compared with the nominal 10 nm XPS information depth. By inverting the K–O range–energy power law within a CSDA, we estimated the fraction of the incident electron energy nominally lost along the trajectory segment corresponding to the first 10 nm below the surface. The irradiated mass was independently calculated using the fixed 10 nm XPS information depth. Full details and limitations of this model-dependent estimate are reported in Supplementary Information SI.3.

3. Results and discussion

Initial structure and chemical state of graphene oxide sheets

SEM and XRD analyses were first used to assess the morphology and structural organization of the self-supported GO sheets. The top-view SEM image of the as-prepared sheet shows a compact wrinkled surface, typical of stacked and partially folded GO sheets (Fig. 1a). After soft X-ray irradiation, the GO sheet preserves a similar micrometre-scale morphology, without evident cracking, delamination or ablation (Fig. 1c). This indicates that the irradiation conditions used in this work mainly induce chemical modifications, as probed by XPS, rather than severe morphological degradation of the GO film. XRD spectra collected on the self-supported sheet before and after irradiation are reported in Fig. 1b and Fig. 1d, respectively.

The XRD pattern of the as-prepared GO sheet exhibits the characteristic GO (002) reflection, confirming the ordered stacking of oxidized graphene layers (Fig. 1b). After irradiation, the (002) reflection is still observed, indicating that the lamellar structure of the GO sheet is largely preserved (Fig. 1d). However, a slight shift of the peak position after irradiation can be observed and suggests a modification of the interlayer spacing, consistent with partial reduction and rearrangement of the GO layers[22]. After irradiation, the GO (002) peak shifted from 11.54° to 12.07°, indicating a decrease in the interlayer spacing according to Bragg's law. The position of the (002) reflection was used to calculate the interlayer distance $d_{(002)}$ through Bragg's law. The resulting $d_{(002)}$ value was then used to estimate the effective structural density of the GO sheet through the empirical density–interlayer spacing relationship reported for GO films[22], as detailed in the Supplementary Information (SI.1). This effective density was used as an input parameter for the absorbed-dose calculation.

The full local absorbed-dose estimation, including the assumptions on probing depth, density, photon attenuation and electron energy loss, is reported in Supplementary Information SI.3. Within this framework, the estimated nominal local dose rate is 5.15 MGy h^{-1} for Mg Kα irradiation and 1150 MGy h^{-1} for 500 eV electron irradiation. For the electron calculation, the irradiated mass was defined by the nominal 10 nm XPS information depth, while the fraction of incident energy assigned to this layer was estimated using a K–O-derived CSDA.

The cross-section SEM images, reported in the same panels, further confirm the lamellar nature of the self-supported sheet, showing a stacked layered structure before and after irradiation.

Radiation-induced evolution of C 1s and O 1s spectra

By means of detailed core-level XPS measurements we compare representative C 1s and O 1s core level peaks of GO sheets before and after irradiation with Mg Kα X-rays (Fig. 2(a) and 2(c)) and 500 eV electrons (Fig. 2(b) and 2(d)). The C 1s spectra of the GO samples showed the typical coexistence of graphitic carbon and oxygenated carbon species, including hydroxyl, epoxide, carbonyl and carboxyl groups. The O 1s region was consistently decomposed into hydroxyl-related, epoxide-related and carbonyl/carboxyl oxygen components. These spectra were used as the reference state for evaluating the chemical evolution induced by irradiation (more details are reported in SI.2).

For both irradiation sources, the spectral evolution of both core-level regions is consistent and indicate a progressive and chemically selective reduction of the GO surface.

In the C 1s region, the most evident spectral change is the decrease of the epoxide C–O–C component at approximately 286.9 eV, together with a relative increase of the graphitic C–C/C = C contribution at approximately 284.8 eV.

The O 1s spectra provide an independent confirmation of this selective evolution. After irradiation, the epoxide-related oxygen component at approximately 532.0 eV decreases markedly, whereas the hydroxyl-related component at approximately 533.4 eV shows a relative increase. By contrast, the lower-binding-energy contribution associated with carbonyl and carboxyl oxygen environments at approximately 530.4 eV varies only slightly. The agreement between the C 1s and O 1s regions strengthens the assignment of epoxide groups as the preferentially affected oxygen functionality and indicates that irradiation promotes both epoxide depletion and partial conversion into hydroxyl-related configurations. This behaviour indicates that the radiation-induced reduction of GO is not a uniform removal of all oxygen-containing groups. Instead, the process selectively affects specific chemical functional groups, with epoxide groups being the most radiation-sensitive species.

Dose-dependent evolution of C 1s components

The quantitative evolution of the C 1s components as a function of absorbed dose is reported in Fig. 3(a,b). The relative intensities of the identified C 1s components were obtained from the complete irradiation series reported in Supplementary Information SI.2. For the two irradiation sources, the epoxide component decreases monotonically with increasing dose, while the graphitic C–C/C = C contribution increases. This opposite trend confirms that the depletion of C–O–C groups is directly associated with the partial restoration of graphitic domains.

The hydroxyl component exhibits a moderate increase, suggesting that irradiation does not simply remove oxygen atoms from the GO surface. A possible contribution may arise from epoxide ring opening followed by local rearrangement into hydroxyl-related configurations. In contrast, carbonyl and carboxyl

species remain nearly constant over the investigated dose range, indicating that these groups are less sensitive to the irradiation conditions used here.

This interpretation is also supported by the O 1s spectra in Fig. 2(c,d), where the loss of the epoxide-oxygen contribution is accompanied by a relative enhancement of hydroxyl-related oxygen, while the carbonyl/carboxyl oxygen component remains comparatively stable. Thus, the oxygen-side analysis corroborates the trends extracted quantitatively from the C 1s fits.

These results identify the epoxide component as the most suitable chemical marker for following the radiation-induced reduction of GO.

Dose-normalized epoxide-depletion kinetics

To compare the chemical response of GO under different irradiation sources, the evolution of the epoxide component was quantified using a dose-dependent XPS reduction yield. The epoxide contribution was normalized to the graphitic carbon component to minimize the effect of possible variations in signal intensity and initial surface oxidation. The epoxide-depletion yield was defined as:

$$Y_D = 100 \times \left[1 - \frac{\left(\frac{A_{C-O-C}}{A_{C-C}}\right)_D}{\left(\frac{A_{C-O-C}}{A_{C-C}}\right)_0}\right] \# \ (3)$$

where $\left(\frac{A_{C-O-C}}{A_{C-C}}\right)_D$ is the epoxide-to-graphitic carbon area ratio after an absorbed dose *D*, and $\left(\frac{A_{C-O-C}}{A_{C-C}}\right)_0$ is the corresponding value before irradiation.

The dose dependence of Y_D was fitted using a first-order-like saturation model:

$$Y_D = Y_\infty \ \left(1 - e^{-D/D_c}\right) \# \ (4)$$

where Y_∞ is the saturation yield, D_c represents the characteristic dose.

Figure 4(a) shows Y_D as a function of the absorbed dose for Mg Kα X-ray irradiation, whereas Fig. 4(b) shows the corresponding results for 500 eV electron irradiation. For both irradiation sources, the dose dependence of Y_D is adequately described by the first order-like saturation model introduced in Eq. (4). This behaviour is consistent with an initially pronounced depletion of radiation-sensitive C–O–C sites, followed by a progressive slowing of the response as their population decreases. The fitted characteristic dose value D_c is 140 ± 10 MGy for Mg Kα X-ray irradiation and 2310 ± 235 MGy for electron irradiation, and the corresponding saturation yields are $\mathrm{Y}_\infty = 74 \pm 3 \backslash \%$ and $\mathrm{Y}_\infty = 72 \pm 5 \backslash \%$, respectively. The fits yielded a parameter $R^2 = 0.997 \backslash$:for both source irradiation. The reported uncertainties represent standard errors obtained from nonlinear regression.

Importantly, for electron irradiation, D_c is higher than the maximum experimentally investigated dose of 2300 MGy. At 2300 MGy dose, the fitted response reaches only approximately 62% of Y_∞ ; therefore, the saturation regime is not experimentally reached. Consequently, the fitted electron Y_∞ and D_c values should be considered model-dependent extrapolated estimates and interpreted with caution. Nevertheless, within the investigated dose range, the substantially higher characteristic dose obtained for electron irradiation is consistent with a lower dose-normalized sensitivity of the epoxide-depletion response compared to irradiation with Mg Kα radiation.

This result highlights the importance of distinguishing between exposure-time kinetics and absorbed-dose-normalized response. Under the maximum exposure conditions, the nominal local electron dose is approximately 13 times the Mg Kα dose within the adopted K–O-derived CSDA approximation (see Supplementary Information for more details). Therefore, the faster real-time evolution observed under electron irradiation mainly reflects the much higher dose rate, whereas the larger electron characteristic dose indicates a lower dose-normalized chemical efficiency. When the response is expressed as a function of absorbed dose, soft X-rays exhibit a higher efficiency in promoting the XPS-detectable depletion of epoxide groups in GO sheets. The different values of D_c likely reflect the depth profiles and interaction mechanisms of photons and low-energy electrons.

Overall, the data demonstrate that epoxide depletion in GO can be described within a common dose-response framework, while the characteristic dose constant remains strongly dependent on the irradiation source.

Mechanistic interpretation and source-dependent response

The preferential depletion of epoxide groups suggests that the radiation-induced reduction process is initiated mainly by bond-breaking events involving the strained C–O–C functionalities. Energy deposition can promote epoxide ring opening, oxygen desorption and local reconstruction of the carbon network, leading to the progressive recovery of sp^2-rich domains. The concomitant increase of hydroxyl-related components suggests that part of the epoxide population may also evolve through intermediate oxygenated configurations rather than being directly removed from the surface. The corresponding decrease of the epoxide component in the O 1s region provides direct oxygen-side evidence for this pathway, while the relative growth of hydroxyl-related oxygen is consistent with epoxide ring opening and local rearrangement before, or in competition with, oxygen desorption.

The different dose-normalized efficiencies observed for soft X-rays and electrons likely reflect their different interaction mechanisms and depth. If only irradiation time is considered when comparing the two irradiation sources, then low-energy electrons seem to induce faster changes as a function of exposure time. However, when the response is normalized to the absorbed dose (that is, considering the absorbed energy and the irradiated mass within the volume probed by XPS), their efficiency is much lower than that of soft X-rays. This may indicate that only a fraction of the electron-deposited energy is effectively converted into epoxide depletion within the XPS-probed surface region, while part of the energy may be redistributed through scattering, secondary-electron emission, charging effects or non-

reductive excitation pathways. Since the K–O formalism provides only an approximate electron range and does not account for the full low-energy electron transport and energy-deposition profile, the electron dose should be regarded as a local physical dose estimate rather than as a direct measure of the chemically effective dose. Part of the apparent difference between the characteristic doses may also arise from the different uncertainty levels associated with the photon and electron dose estimates, particularly from the low-energy extrapolation of the K–O relation and the simplified treatment of electron energy deposition.

Within the investigated dose range, the initial increase of Y_D provides a sensitive basis for comparing the early-stage chemical response of GO to the two radiation sources. However, the marked difference between the fitted characteristic doses demonstrates that epoxide depletion cannot be interpreted as a source-independent function of the estimated local absorbed dose. Instead, D_c should be regarded as a phenomenological parameter that describes the response under the specific irradiation and energy-deposition conditions considered here.

4. Conclusion

A systematic XPS investigation of self-supported GO sheets exposed to soft X-rays (Mg Kα) and low-energy electrons (500 eV) reveals a common irradiation-induced reduction pathway dominated by selective epoxide depletion. Notably, the C 1s and O 1s spectra show that irradiation decreases the C–O–C contribution, while graphitic C–C/C = C and hydroxyl-related components increase. Carbonyl and carboxyl groups remain comparatively stable over the investigated exposure range, demonstrating that the chemical evolution is selective rather than a uniform loss of oxygen-containing species.

The epoxide-depletion yield, defined from the normalized decrease of the C–O–C/C–C area ratio, follows a first-order-like saturation trend as a function of the estimated local absorbed dose for both radiation sources. Nevertheless, the substantially different characteristic doses show that the response is source dependent. The characteristic dose is approximately 140 MGy for soft X-rays and 2310 MGy for electrons.

Apparently, if only the irradiation time is considered, it seems that electrons are more effective than X-ray in inducing GO reduction. However, Within the adopted model-dependent local-dose estimate, soft X-rays exhibit a higher apparent dose-normalized efficiency for XPS-detectable epoxide depletion than 500 eV electrons. Indeed, the nominal local electron dose is approximately 13 times the Mg Kα dose within the adopted K–O-derived CSDA approximation. This difference indicates that the local physical dose estimate is not, by itself, a source-independent measure of the energy effectively driving epoxide depletion. Source-specific interaction mechanisms, scattering, secondary-electron emission, charging and near-surface energy-deposition profiles may all contribute to the observed behaviour.

These results establish epoxide depletion as a chemically selective descriptor of irradiation-induced GO reduction. The qualitatively similar evolution observed under the two sources, together with their markedly different characteristic doses, demonstrates that the chemical response is governed not only

by the amount of absorbed dose but also by the type of the radiation source and its characteristics interaction mechanism and energy-deposition volume.

Declarations

Competing interests

The authors declare no competing interests.

Funding

This research received no external funding.

Author Contribution

E.F. and D.C. performed the experiments and analysed the XPS data. L.C. and L.L. contributed to data interpretation and validation. M.P. conceived and supervised the study. All authors discussed the results, contributed to writing the manuscript and approved the submitted version.

Data Availability

The datasets generated and analysed during the current study are available from the corresponding author on reasonable request.

References

1. Dreyer, D. R., Park, S., Bielawski, C. W. & Ruoff, R. S. The chemistry of graphene oxide. *Chem. Soc. Rev.* **39**, 228–240 (2010).
2. Eda, G. & Chhowalla, M. Chemically derived graphene oxide: towards large-area thin-film electronics and optoelectronics. *Adv. Mater.* **22**, 2392–2415 (2010).
3. Aliyev, E. et al. Structural characterization of graphene oxide: surface functional groups and fractionated oxidative debris. *Nanomaterials* **9**, 1180 (2019).
4. Pei, S. & Cheng, H. M. The reduction of graphene oxide. *Carbon* **50**, 3210–3228 (2012).
5. de Barros, N. G. et al. Graphene oxide: a comparison of reduction methods. *C* **9**, 73 (2023).
6. Imae, I. Reduction of graphene oxide using an environmentally friendly method and its application to energy-related materials. *Coatings* **11**, 297 (2021).
7. Gomez-Mancebo, M. B. et al. Comparison of thermal and laser-reduced graphene oxide production for energy storage applications. *Nanomaterials* **13**, 1391 (2023).

8. Prezioso, S. et al. Dose and wavelength dependent study of graphene oxide photoreduction with VUV Synchrotron radiation. *Carbon* **79**, 478–485 (2014).
9. Abou Zeid, S. et al. Radiation induced reduction of graphene oxide: a dose effect study. *New J. Chem.* **48**, 4749–4764 (2024).
10. Goncalves, M. G. et al. Functionalization of graphene oxide via epoxide groups: a comprehensive review of synthetic routes and challenges. *Front. Carbon*. **3**, 1393077 (2024).
11. Kovtun, A. et al. Accurate chemical analysis of graphene-based materials using X-ray photoelectron spectroscopy. *Carbon* **143**, 268–275 (2019).
12. Rabchinskii, M. K. et al. Manifesting epoxide and hydroxyl groups in XPS spectra and valence band of graphene derivatives. *Nanomaterials* **13**, 23 (2023).
13. Hufner, S. *Photoelectron Spectroscopy* (Springer, 2003). 10.1007/978-3-662-09280-4
14. Seah, M. P. & Dench, W. A. Quantitative electron spectroscopy of surfaces: a standard data base for electron inelastic mean free paths in solids. *Surf. Interface Anal.* **1**, 2–11 (1979).
15. Tanuma, S., Powell, C. J. & Penn, D. R. Calculations of electron inelastic mean free paths. IX. Data for 41 elemental solids over the 50 eV to 30 keV range. *Surf. Interface Anal.* **43**, 689–713 (2011).
16. Di Crescenzo, A. et al. Graphene oxide foils as an osteoinductive stem cell substrate. *ACS Appl. Bio Mater.* **2**, 1643–1651 (2019).
17. Henke, B. L., Gullikson, E. M. & Davis, J. C. X-ray interactions: photoabsorption, scattering, transmission, and reflection at E = 50–30000 eV, Z = 1–92. *At. Data Nucl. Data Tables*. **54**, 181–342 (1993).
18. Kanaya, K. & Okayama, S. Penetration and energy-loss theory of electrons in solid targets. *J. Phys. D*. **5**, 43–58 (1972).
19. Drouin, D. et al. CASINO V2.42: A fast and easy-to-use modeling tool for scanning electron microscopy and microanalysis users. *Scanning* **29**, 92–101 (2007).
20. Nuclear Energy & Agency *PENELOPE 2018: A Code System for Monte Carlo Simulation of Electron and Photon Transport* (OECD Publishing, 2019). 10.1787/32da5043-en
21. Allison, J. & others. Recent developments in Geant4. *Nuclear Instruments and Methods in Physics Research Section A: Accelerators, Spectrometers, Detectors and Associated Equipment* 835, 186–225 (2016).
22. Jimenez Rioboo, R. J. et al. Elastic constants of graphene oxide few-layer films: correlations with interlayer stacking and bonding. *J. Mater. Chem. C*. **3**, 4868–4875 (2015).

Figures

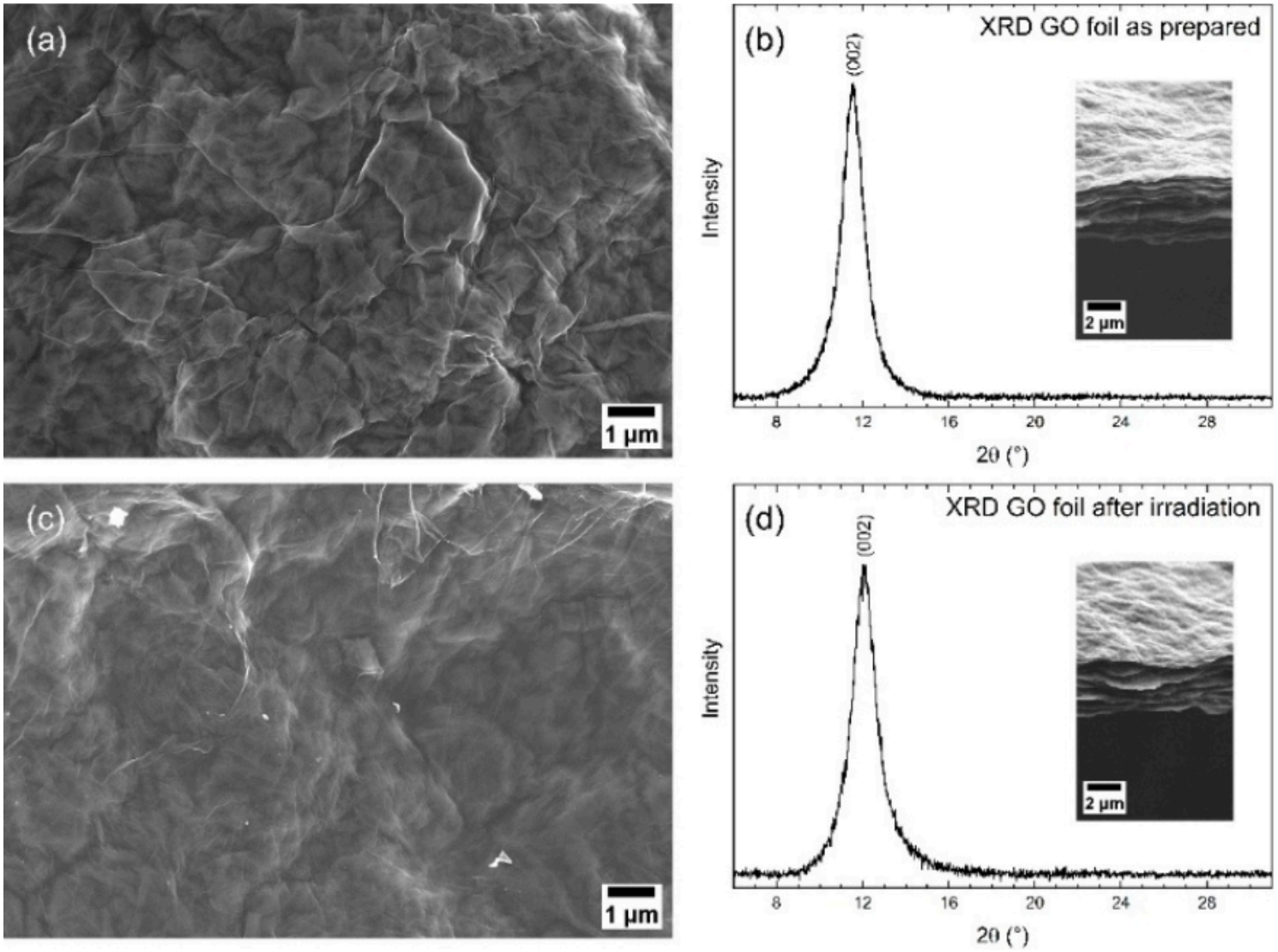


Figure 1

(a) Top-view SEM image of the as-prepared GO sheet, showing a compact wrinkled morphology typical of stacked and partially folded GO sheets. (b) XRD pattern of the as-prepared GO sheet, showing the characteristic GO (002) reflection; the inset reports an edge-view SEM image highlighting the stacked lamellar structure of the sheet. (c) Top-view SEM image of the GO sheet after irradiation, showing that the micrometre-scale morphology is preserved, without evident cracking, delamination or ablation. (d) XRD pattern of the GO sheet after irradiation; the persistence of the GO (002) reflection indicates that the lamellar structure is retained after exposure, while the change in peak position reflects a modification of the interlayer spacing. The $d_{(002)}$ values extracted from the XRD patterns were used to estimate the effective structural density of the GO sheet for the absorbed-dose calculation. Scale bars are 1 µm in panels (a,c) and 2 µm in the SEM insets of panels (b,d).

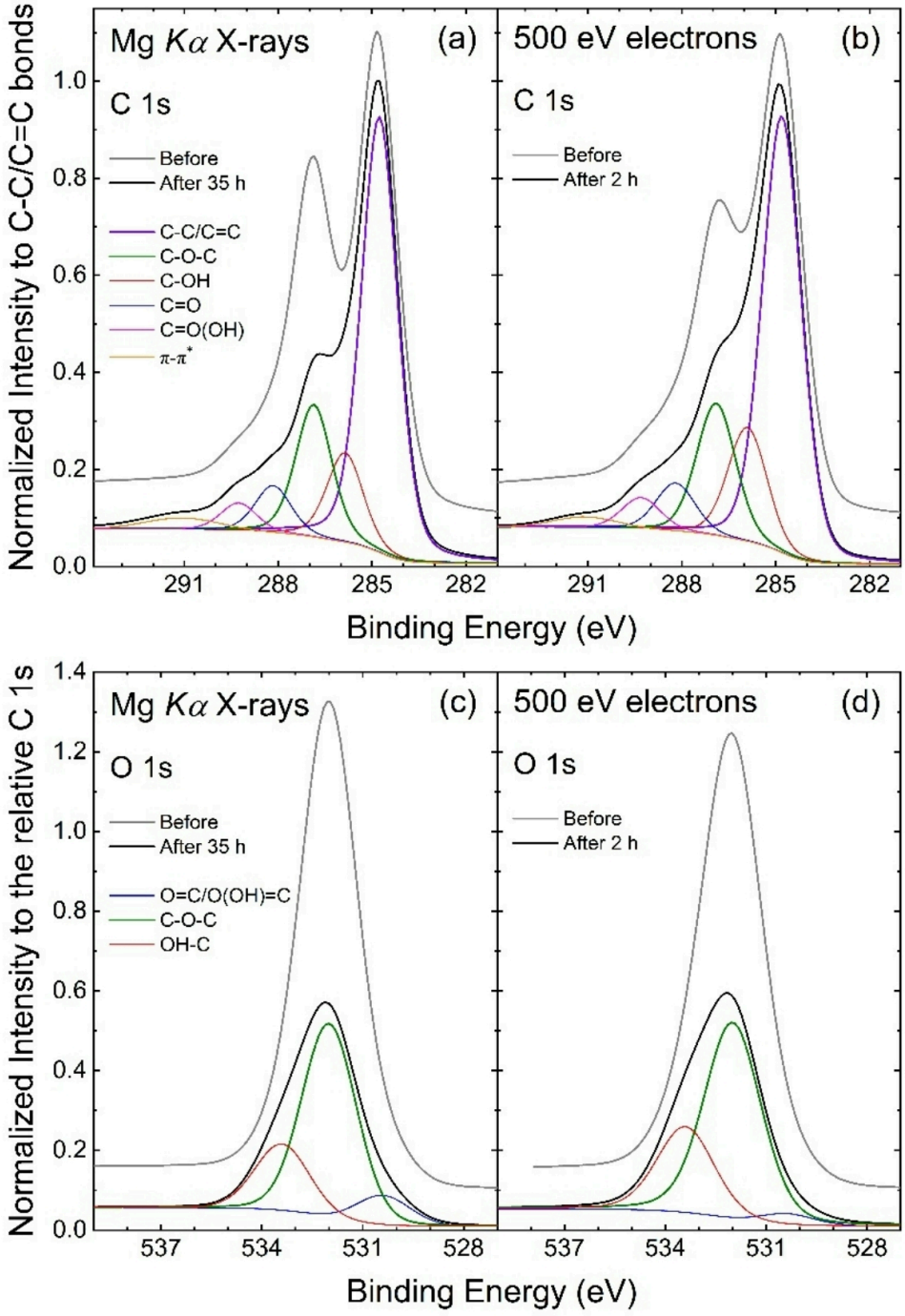


Figure 2

Radiation-induced evolution of the C 1s and O 1s XPS spectra of graphene oxide. Representative normalized spectra of GO before (gray line) and after irradiation (black line) with Mg Kα X-rays for 35 h and 500 eV electrons for 2 h are shown for the C 1s and O 1s energy regions. The C 1s spectra are normalized to the graphitic C–C/C=C component, while the O 1s spectra are normalized to the corresponding C 1s signal. Continuous curves represent the fitted components of the irradiated spectra.

The C 1s fits include graphitic carbon C–C/C=C (purple line), hydroxyl C–OH (red line), epoxide C–O–C (green line), carbonyl C=O (blue line), carboxyl O–C=O (magenta line) and the π–π* shake-up contribution (orange line). The O 1s fits include hydroxyl-related oxygen (red line), epoxide oxygen (green line) and carbonyl/carboxyl oxygen (blue line) environments. For both irradiation sources, the decrease of the epoxide-related contribution in the C 1s and O 1s regions, together with the increase of graphitic carbon and the relative enhancement of hydroxyl-related oxygen, confirms the selective reduction of the GO surface.

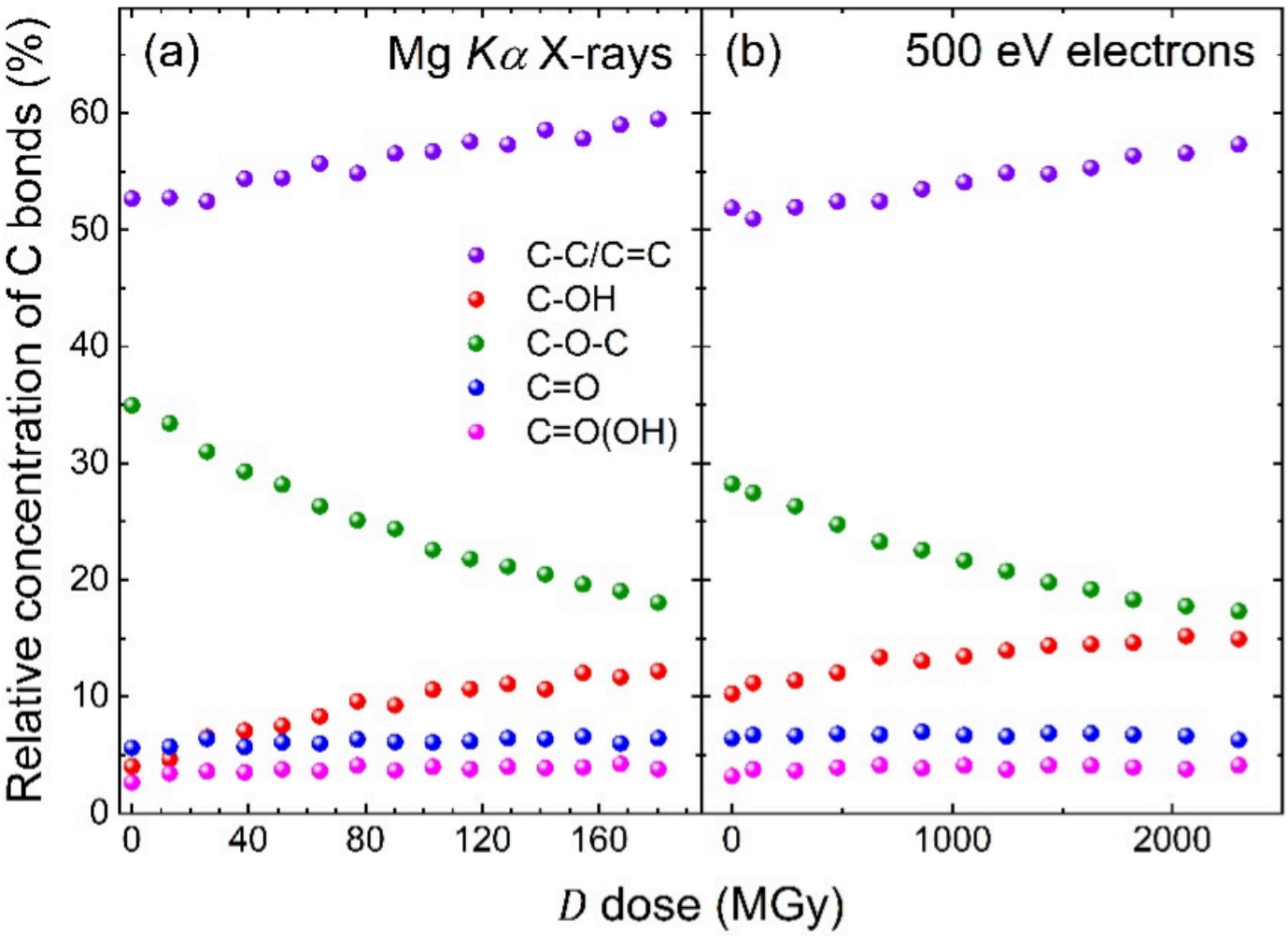


Figure 3

Relative concentration of each C 1s component extracted from the XPS fitting procedure as a function of absorbed dose for (a) Mg Kα X-ray irradiation and (b) 500 eV electron irradiation. The epoxide C–O–C component decreases monotonically with increasing dose, whereas the graphitic C–C/C=C component progressively increases. Hydroxyl-related species show a moderate increase, while carbonyl and carboxyl contributions remain nearly unchanged over the investigated dose range. This selective evolution identifies epoxide groups as the most radiation-sensitive chemical sites in GO.

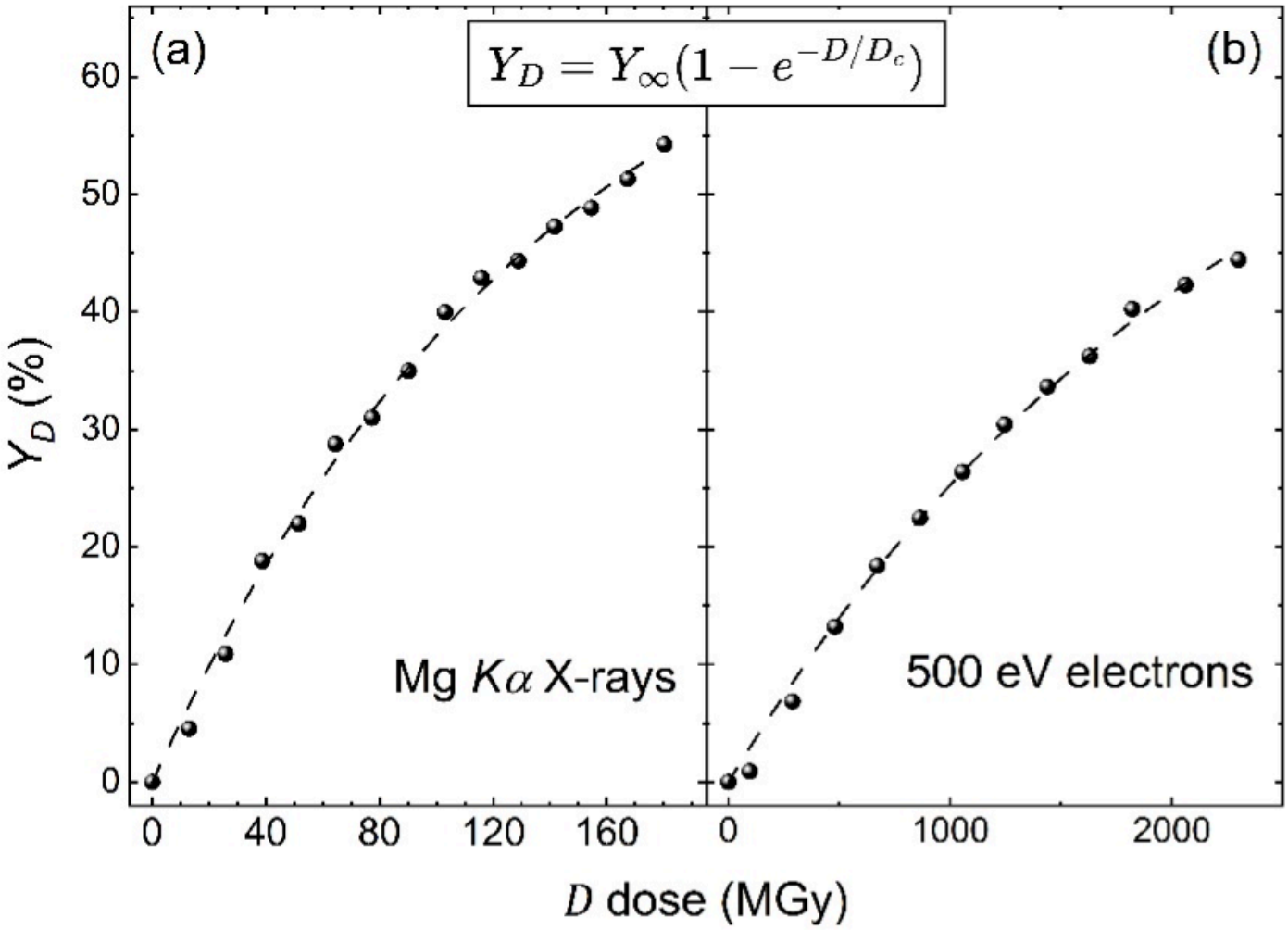


Figure 4

Epoxide-depletion yield Y_D, defined from the normalized decrease of the C–O–C/C–C area ratio, as a function of absorbed dose for (a) soft X-ray irradiation using Mg Kα photons and (b) 500 eV electron irradiation. Dashed lines represent fits performed using the first-order-like saturation model introduced in Eq. (4). Both datasets are adequately described by the same dose-response model, although the saturation regime is not experimentally reached for electron irradiation. Within the investigated dose range, the electron-induced response exhibits a lower apparent dose-normalized sensitivity than the Mg Kα-induced response.

Supplementary Files

This is a list of supplementary files associated with this preprint. Click to download.

- GOScientificReportsSI.docx